Geothermics 57 (2015) 246–257

Contents lists available at ScienceDirect

Geothermics

journal homepage: www.elsevier.com/locate/geothermics

Resistivity characterization of the Krafla and Hengill geothermal fields through 3D MT inverse modeling

Erika Gasperikova[a,*], Gudni K. Rosenkjaer[b,c], Knutur Arnason[b], Gregory A. Newman[a], Nathaniel J. Lindsey[a]

[a] Lawrence Berkeley National Laboratory, 1 Cyclotron Road, MS74R316C, Berkeley, CA 94720, United States
[b] ISOR Iceland GeoSurvey, Grensasvegur 9, 108 Reykjavik, Iceland
[c] University of British Columbia, 6339 Stores Road, Vancouver, BC, Canada V6T 1Z4

ARTICLE INFO

Article history:
Received 25 November 2014
Received in revised form 17 June 2015
Accepted 20 June 2015
Available online 13 July 2015

Keywords:
Magnetotellurics
3D inversion
Geothermal
Iceland
Krafla
Hengill

ABSTRACT

Krafla and Hengill volcanic complexes, located 300 km apart, are both known as high-temperature geothermal systems located within neo-volcanic zones of Iceland. This paper demonstrates the utilization of three-dimensional (3D) magnetotelluric (MT) inversions from three different inverse modeling algorithms, which leads to characterizing the electrical resistivity structure of geothermal reservoirs with a much greater level of confidence in accuracy and resolution than if a single algorithm was employed in the data interpretation. These are the first 3D MT inversions of a Krafla MT dataset. The inverted model of electrical resistivity is a classic example of a high-temperature hydrothermal system, with a highly resistive near-surface layer, identified as unaltered porous basalt, overlying a low resistivity cap corresponding to the smectite–zeolite zone. This layer is in turn underlain by a more resistive zone, identified as the epidote–chlorite zone, also called the resistive core, which is often associated with production of geothermal fluids. The electrical structure in the upper 1–2 km does not correlate with lithology but with alteration mineralogy. At the location of the IDDP-1 well, which encountered magma at 2.1 km depth, the resistivity image shows high resistivity, most likely due to the epidote–chlorite geology and the presence of deeper superheated or supercritical fluids. Two km northwest of the well, however, an intrusive low-resistivity feature is imaged rising from depth, and a plausible interpretation is that of a magma intrusion. One possible explanation for the magma encounter at the IDDP-1 well is the existence of pathways or fissures connected to the magma chamber and intersected by the well. The MT response to these magma pathways is not discernible in the existing data, perhaps because this magma volume is below the threshold of resolvability. The electrical resistivity structure of the Hengill geothermal area also reveals characteristic features of a high temperature geothermal system with two low-resistivity layers. The nature of the uppermost low-resistivity layer and the increasing resistivity below it is attributed to hydrothermal mineral alteration, while the nature of the deep low-resistivity layer, centered over the northeast, is not yet well understood. The geothermal system in the northeast area appears to be shallower than the system manifested in the southwest. 3D MT inversions of Krafla and Hengill data sets show that knowledge of the subsurface electrical resistivity contributes substantially to a better understanding of complex geothermal systems.

1. Introduction

A critical component in understanding the properties of complex geothermal reservoirs, specifically those typical of Iceland, is the ability to provide images of the subsurface structures that control geothermal fluid flow. Electrical resistivity is a primary physical property of the Earth, one which is strongly influenced by hydrothermal processes present in geothermal reservoirs. If mapped, resistivity can be used to infer untapped fracture systems and regions of increased permeability and fluid content, as well as conductive alteration of minerals (clays, etc.) due to natural or induced fracturing arising from hydraulic stimulation of the reservoir. Magnetotellurics (MT) has a long history in geothermal exploration. The classic MT response of a high temperature reservoir shows resistivity as an indirect indicator of geothermal fluids, as a response to clay-alteration mineralogy (Pellerin et al., 1996).

* Corresponding author..
E-mail address: egasperikova@lbl.gov (E. Gasperikova).

http://dx.doi.org/10.1016/j.geothermics.2015.06.015
0375-6505/

However, fluids might not be present if the system is fossilized. 3D MT modeling and inversion has emerged as a promising technique to model and image geothermal reservoirs in a self-consistent manner, to the level supported by field data accuracy and resolution. In this paper, MT data acquired over the Krafla and Hengill geothermal fields in Iceland are analyzed and interpreted using 3D inverse modeling. Three different modeling codes are used to better appraise the quality and resolution of the 3D resistivity images (Rosenkjaer et al., 2015), resulting in a greater degree of confidence in the 3D interpretation of the MT data.

2. MT data analysis and inversion

MT uses naturally occurring broadband electromagnetic (EM) fields over the Earth's surface to image the electrical resistivity structure of the Earth. These EM fields arise from regional and worldwide thunderstorm activity, and from interaction of the solar wind with the Earth's magnetosphere. These sources are remote and have a high index of refraction at the air–Earth interface; hence, the EM fields at the surface of the Earth behave almost like plane waves, and propagate vertically into the Earth. The amplitude, phase, and directional relationship between electric (E) and magnetic (H) fields on the surface depend on the subsurface distribution of electrical resistivity. Furthermore, the waves are arbitrarily polarized over a 3D Earth, which requires vector measurements of the EM fields and a tensor formulation to completely represent the subsurface electrical resistivity structure (Madden and Nelson, 1986).

The horizontal components of E and H fields (E_x, E_y, H_x, H_y) are interrelated by

$$\begin{pmatrix} E_x \\ E_y \end{pmatrix} = \begin{pmatrix} Z_{xx} & Z_{xy} \\ Z_{yx} & Z_{yy} \end{pmatrix} \begin{pmatrix} H_x \\ H_y \end{pmatrix}$$

where the surface impedance Z is a 2×2 tensor, obtained for each MT recording station as a function of frequency, denoted by the symbol f. Apparent resistivity and impedance-phase quantities, which are more intuitive to inspect and interpret (Vozoff, 1991), can be readily obtained by manipulating the elements of the impedance tensor components. For the xy-component, for example, the ratio of E_x to H_y is proportional to $\sqrt{\rho}$, where ρ is resistivity, and the phase of Z is the difference between the phases of E and H. The apparent resistivity is then

$$\rho_{xy} = \frac{1}{\mu\omega}\left|\frac{E_x}{H_y}\right|^2,$$

where $\omega = 2\pi f$ is the angular frequency, and μ is magnetic permeability.

Similar relationships hold for all other components of the impedance matrix.

MT data acquired at both Krafla and Hengill geothermal fields span frequencies from 0.001 to 300 Hz. Rosenkjaer et al. (2015) describe data processing and three 3D inversion codes that were used for the inversion: model space inversions – (1) MT3Dinv (Farquharson et al., 2002), (2) EMGeo (Newman and Alumbaugh, 2000; Newman et al., 2003), and (3) a data domain inversion algorithm WSINV3DMT (Siripunvaraporn, 2011). Our ultimate aim is to construct 3D resistivity models of the geothermal systems in the studied areas to better understand their structure. In this paper, while results of all three inversion codes are presented, for clarity of interpretation, we will often show results from one inversion code for each area only, because the other two codes recovered similar structures to those reported here. Rosenkjaer et al. (2015) compares the recovered models and uses additional parameters that might be useful in an appraisal of the resulting resistivity models. Examples of data fits of all three codes in the Krafla area are shown in Fig. 1b, with station locations shown in Fig. 1a. Data fits for all three codes in the Hengill area are shown in Fig. 2b, with station locations in Fig. 2a.

Both sets of examples are located in areas of interest and are representative of the majority of the data fits. The areas where the fits are worse or the inversions recover different resistivity structures are discussed in Rosenkjaer et al. (2015). Figs. 1b and 2b illustrate that the Hengill data are better fit by the final models than the Krafla data. Fig. 1b shows that the fit for Station 5 is worse than for Station 3, even though they are very close to each other, which suggests that more noise is present in the Station 5 data. All three codes, however, show the same general behavior at each station, e.g., they all fit or do not fit the data. In general, larger data misfits are observed in the mid-frequency range. Hengill data are more consistent, and all three inversion codes have comparable data misfit levels, although the resulting inversion model from data domain inversion is considerably different from model-based inversions, which are very close to each other as shown in Rosenkjaer et al. (2015). The apparent resistivity and phase curves for the WSINV3DMT code in Fig. 2b are different because this inversion was run with the grid and data aligned to N30°E, while the other two codes used data and grid oriented to the north.

3. Krafla geothermal area

The Krafla volcanic system is located in the northern neovolcanic zone of Iceland (Elders et al., 2011). Significant crustal deformation along a divergent plate boundary, where strain accumulated for more than two centuries, occurred during the Krafla rifting episode of 1975–1989. This episode involved a sequence of magmatic and tectonic events along the plate boundary in northern Iceland and was accompanied by the largest earthquake sequence so far recorded along the divergent plate boundaries of the Atlantic (Einarsson, 1986). The Krafla central volcano has a long history of episodic, predominantly tholeiitic, volcanic activity, with 10–20 years long episodes occurring every 250–1000 years. It has a caldera within the neovolcanic rift system crosscut by an active fissure swarm that extends tens of kilometers in a NNE-SSW direction and includes an ESE-WNW transform faults. Hydrothermal manifestations are controlled by tectonic fractures, faults, and dykes (Fridleifsson et al., 2006). This episodic volcanic activity could also impact the hydrothermal system by opening up new fractures via rifting and injection of magmatic gases, mainly carbon dioxide and hydrogen sulfide. Thus, the rifting process can change the fluid flow regimes, while the magmatic gases can change the composition of the hydrothermal fluids.

The Krafla geothermal area is generally divided into five different well fields (Fig. 3), mainly on the basis of different fluid chemical composition, temperature, and pressure. The oldest well fields, Leirbotnar and Vitismor, lie to the west of the Hveragil gully. The Sudurhlidar well field lies on the south flanks of Mt. Krafla; the Vesturhlidar well field is on the northeastern flanks of the mountain. A fifth field, the Hvitholar, is located ~2 km south of the other four; see Fig. 3 for precise locations of the fields.

Fig. 3 also shows elevations in the 13 km × 10 km study area of the Krafla volcanic system, along with the locations of MT soundings (purple symbols) used in the 3D MT inversions. The white triangle indicates the location of the IDDP-1 (Iceland Deep Drilling Programme) well. MT data were acquired during 2004–2006 campaigns by several research groups. For more detailed data processing and inversion analysis, see Rosenkjaer et al. (2015).

This is the first 3D MT inversion of a Krafla MT dataset – previous interpretation of these MT data was done in one-dimension only (Arnason et al., 2009; Fridleifsson et al., 2014). Fig. 4a shows a

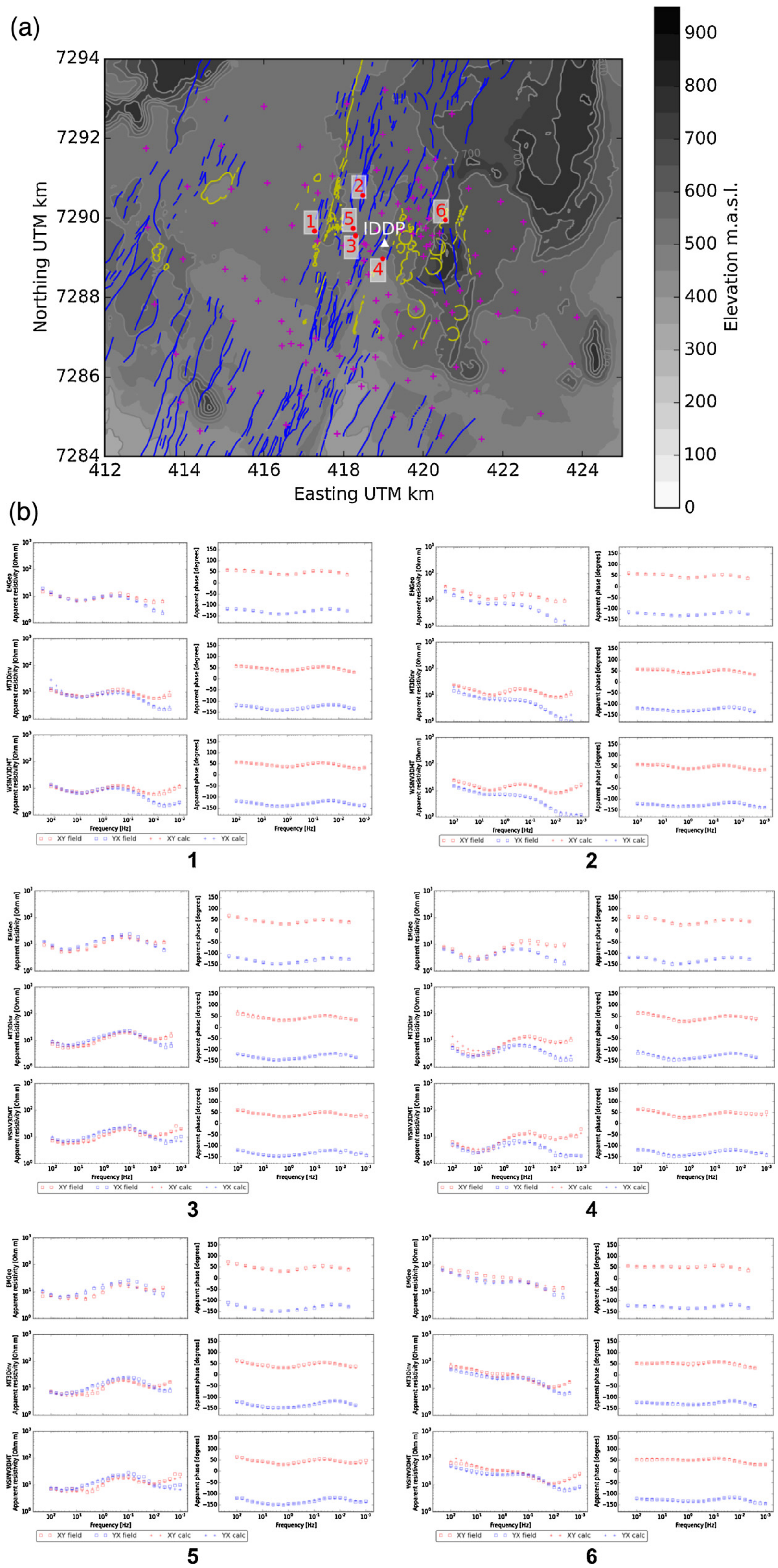

Fig. 1. (a) MT station locations (red symbols with numbers 1–6) at Krafla for data fits shown in (b). Dark blue lines show mapped faults, volcanic features and fissures are shown in yellow, MT site locations are shown as purple plus symbols, and the IDDP-1 well location is indicated by white triangle. (b) Data fits for three inversion codes for MT stations shown in (a); *xy*-mode is plotted in red, *yx*-mode is plotted in blue, field data are plotted using square symbols, calculated data are shown as pluses. For each station, apparent resistivity plot is on the left and phase plot on the right; EMGeo is on the top, MT3Dinv in the middle and WSINV3DMT on the bottom.

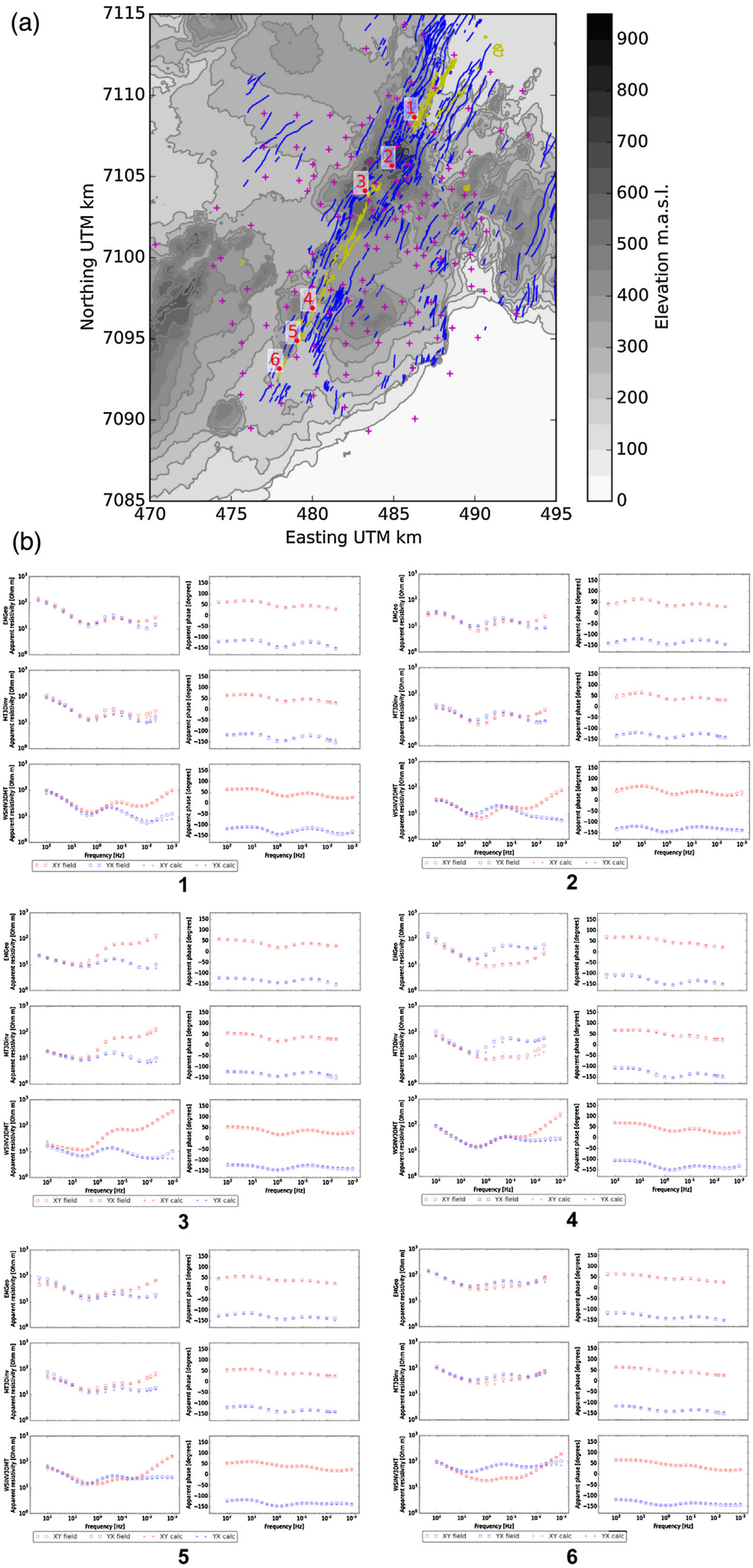

Fig. 2. (a) MT station locations (red symbols with numbers 1–6) at Hengill for data fits shown in (b). Dark blue lines show mapped faults, fissures are shown in yellow, and MT site locations are shown as purple plus symbols. (b) Data fits for three inversion codes for MT stations shown in (a); *xy*-mode is plotted in red, *yx*-mode is plotted in blue, field data are plotted using square symbols, calculated data are shown as pluses. For each station, apparent resistivity plot is on the left and phase plot on the right; EMGeo is on the top, MT3Dinv in the middle and WSINV3DMT on the bottom.

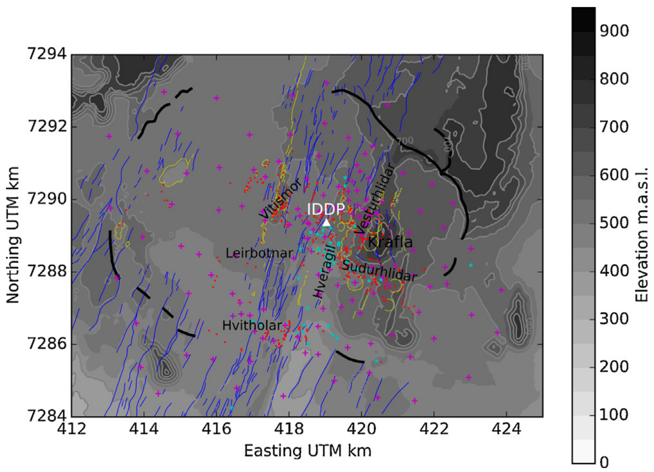

Fig. 3. Krafla elevation map with the IDDP-1 well (white triangle) location, MT site (purple plus symbols) locations and labeled well fields. Dark blue lines show mapped faults, volcanic features and fissures are shown in yellow, and cyan stars are wells drilled in the area. Red circles are surface geothermal manifestations. Krafla caldera is outlined by a thick black line.

cut-away view along and perpendicular to the fissure swarm direction of the 3D resistivity model recovered by the EMGeo inversion (left color scale), along with measured temperatures in drilled wells (right color scale) and mapped faults (brown lines). The resistivity cross-sections along these two directions from all three inversions are shown in Figs. 5 and 6 of Rosenkjaer et al. (2015). The zoom for the area around the wells south of Krafla is shown in Fig. 4b. Fig. 5 shows a 3D resistivity cut-away view at the IDDP-1 well (black vertical line), while Fig. 6 shows a 3D resistivity cut-away view 2 km to the west of the IDDP-1 well, as imaged by WSINV3DMT inversion.

The models of electrical resistivity (Figs. 4–6) reveal a resistive near-surface layer (blue colors), identified as unaltered porous basalts, which covers a low resistivity clay cap (red colors) corresponding to the smectite–zeolite zone. The resistivity of the cap increases with temperature (green and light blue colors) due to the presence of epidote and chlorite until a core of high resistivity is reached (Arnason et al., 2010). The transition from the low resistivity cap to the high-resistivity core coincides with a change in mineral alteration, i.e. from the high CEC smectite and zeolites to the low CEC mixed layered clays, chlorite and epidote – with surface and pore fluid conduction.

In the upper 1–2 km, resistivity does not correlate with lithology but rather with alteration mineralogy (Oskooi et al., 2005). Resistivities below that depth depend on rock types, temperature and a presence of fluids or steam. While the presence of fluids lowers the resistivity, supercritical fluids or steam increase the resistivity (e.g. Spichak and Zakharova, 2014). The resistive core represents not only the transition area identified by the mineral alteration, but also underlying reservoir rocks. Basaltic rocks with superheated steam or supercritical fluids would also have high resistivities. The deep low-resistivity zone appears to be connected to a shallow structure through vertical structures, or "chimneys" (Fig. 6). These low-resistivity structures are located in the same areas as Einarsson (1978) inferred magma chambers manifested at 3–7 km depth by an S-wave shadow zone.

Fig. 4b shows a good correlation between resistivity and temperatures that correspond to different alteration stages at the shallow part of the profile south of Krafla. Temperatures below 100 °C (blue color) correspond to no or very low alteration (high resistivity), 100–200 (220) °C (light blue and white color) correspond to the smectite–zeolite zone (low resistivity), 200–250 °C (dark red color) show the zone where smectite is transformed into chlorite in a transition zone, also called the mixed layer clay zone (increasing resistivity), and above 250 °C (magenta colors) represent chlorite and chlorite–epidote zones (high resistivity).

The IDDP-1 well at Krafla encountered magma at a depth of 2.1 km, and drilling was stopped. The well is located on the flank of the resistive zone with epidote–chlorite alteration and with low-resistivity structures on both sides (Figs. 5 and 6), all running in the NNE-SSW direction, which is consistent with the fissure swarm direction. In this case, the MT measurements show sensitivity to large geological structures, but likely lack sensitivity to individual fractures that are filled with magma or other fluids but not above the volumetric threshold (given their depth). A plausible interpretation of the low-resistivity feature to the NW of the IDDP-1 well, the area of 1975–1984 Krafla fires associated with rifting and volcanic events during that period (Einarsson, 1991), is that of a magma intrusion that goes down to ~5 km depth (Fig. 6) and can be caused by partial melt and/or a brittle-ductile boundary at subsolidus temperatures (Fridleifsson et al., 2014). This intrusion is recovered by all three inversions (see Fig. 5 in Rosenkjaer et al., 2015). Mortensen et al. (2010) suggested that, together with shallow magma chambers, basaltic intrusions below 1–1.5 km release enough heat not only to cause partial melting of hydrated basaltic rocks at shallow depths, but also to cause superheated conditions within the reservoir. Geothermal reservoir temperatures exceed 300 °C at depths as shallow as 2 km (Fig. 4). While models might still be speculative, because of the limited data available, the models by Axelsson et al. (2014) show that a magmatic intrusion could have been emplaced in the vicinity of the IDDP-1 well 25–35 years ago, and the size of it would depend on the distance to the well. No direct contact with the magma was needed to explain relatively high steam temperatures at the well.

Fridleifsson et al. (2014) describe the IDDP-1 site selection process in detail. 1D MT inversion results and micro-seismic data, together with information from two new production wells (K-35 and K-36) and proximity of the existing power plant were considered and prioritized with respect to probability of success. One possible explanation for the magma encountered at the IDDP-1 well is the existence of pathways or fissures connecting the shallow magma chamber to the well. Fridleifsson et al. (2014) show that geology in the vicinity of the IDDP-1 well is changing on a scale not resolvable with existing MT data. For example, well K-25, less than 100 m away and of almost equal depth, did not intersect magma. As also described in Fridleifsson et al. (2014), two Holocene volcanic fissures were intersected at 1.6 and 2.3 km depths in the wells east of the IDDP-1. It should be noted that encounters of unsolidified magma in geothermal wells are extremely rare. The only other documented magma flow into a geothermal well while drilling was in the Puna geothermal field in Hawaii at ~2.5 km depth. Well K-39, ~2 km southeast of the IDDP-1, recovered silicic glass at ~2.5 km depth, where the temperature was 386 °C (Mortensen et al., 2010).

At Vitismor and northwest of it, the low resistivity at the depth of 3.5–6 km does not extend to the south or east. The shallow low-resistivity anomaly SE of the junction of Leirbotnar, Hveragil and Sudurhlidar extends to a depth of ~1.5 km, which is several hundred meters deeper than in the other three areas. A similar shallow low-resistivity response is present northeast of Hvitholar and under Vesturhlidar at ~1–2 km depth. The high resistivities clearly outline the caldera (black line in Figs. 5 and 6) on the west and east flanks. The structure is much more complicated in the southeast part, where the fissure swarm cuts through the caldera.

4. Hengill geothermal area

The Hengill volcanic complex is located about 30 km southeast of Reykjavik at a triple junction of the American-Eurasian plate

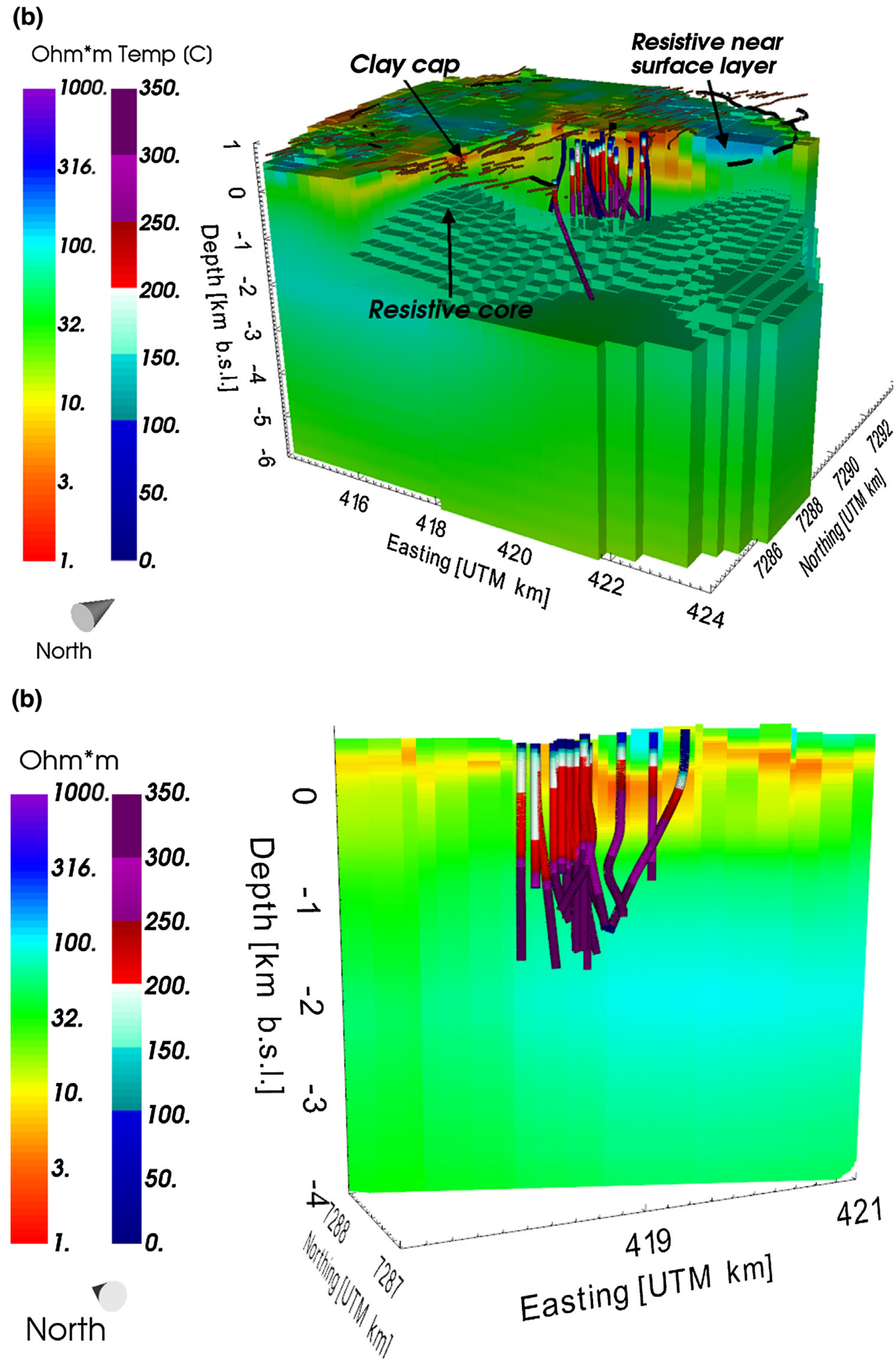

Fig. 4. (a) EMGeo 3D resistivity model of the Krafla geothermal area. (b) NW-SW resistivity cross-section from EMGeo 3D model and well temperatures across the area south of Krafla.

boundary between the Western Iceland volcanic zone (an axial rift zone), the Reykjanes Peninsula (an oblique spreading ridge), and the South Iceland seismic zone (a seismically active transform zone) (Foulger and Toomey, 1989). It is considered to be one of the largest high-temperature geothermal areas in Iceland. Hengill has eight production fields, from which the four main production fields are Hellisheidi, Nesjavellir, Bitra and Hverahlid (Fig. 7).

The Hengill geothermal system is formed by the percolation of groundwater from the heat source at the base of the central volcano, with subsequent upflow of geothermal fluid moving toward the southwest and northeast, along the dykes and fissures, feeding Hellisheidi and Nesjavellir geothermal systems (Franzson et al., 2010). Reservoir temperature ranges from 200 to 340 °C. Structurally, the Hengill system is dominated by NE-SW striking faults and fissures that serve as major permeable structures of the hydrothermal system. These are intersected by easterly striking features which may also play a role in the permeability of the geothermal field (e.g., Arnason and Magnusson, 2001; Hardarson

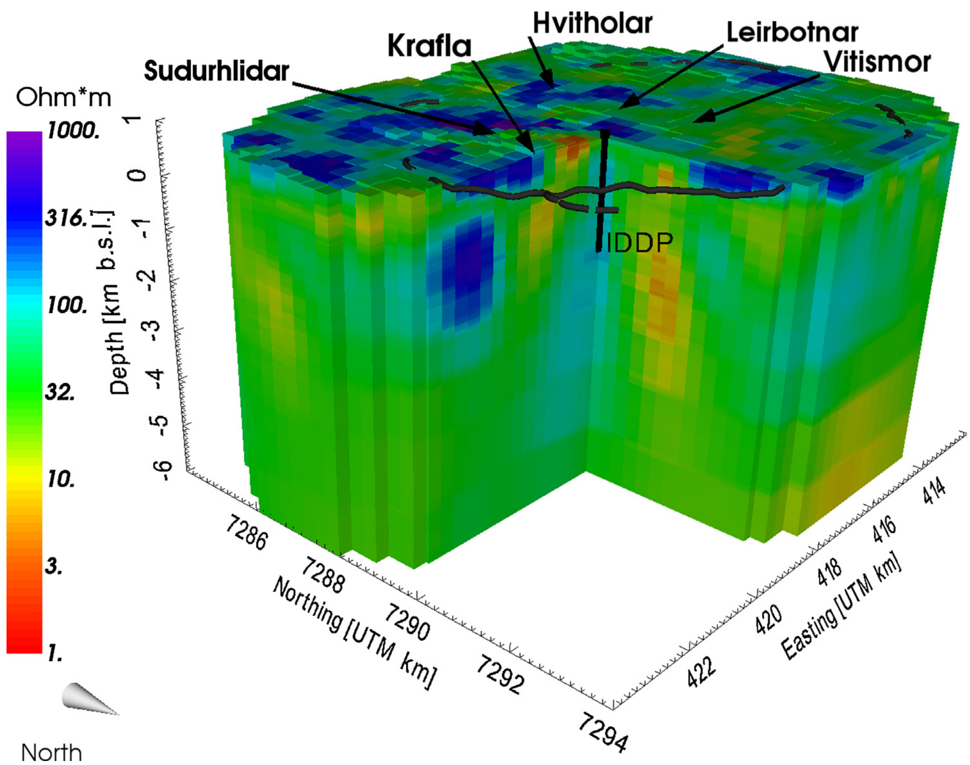

Fig. 5. 3D resistivity cut-away view at the IDDP-1 well location (Easting = 419,033 m and Northing = 7,289,380 m) from the WSINV3DMT 3D resistivity model.

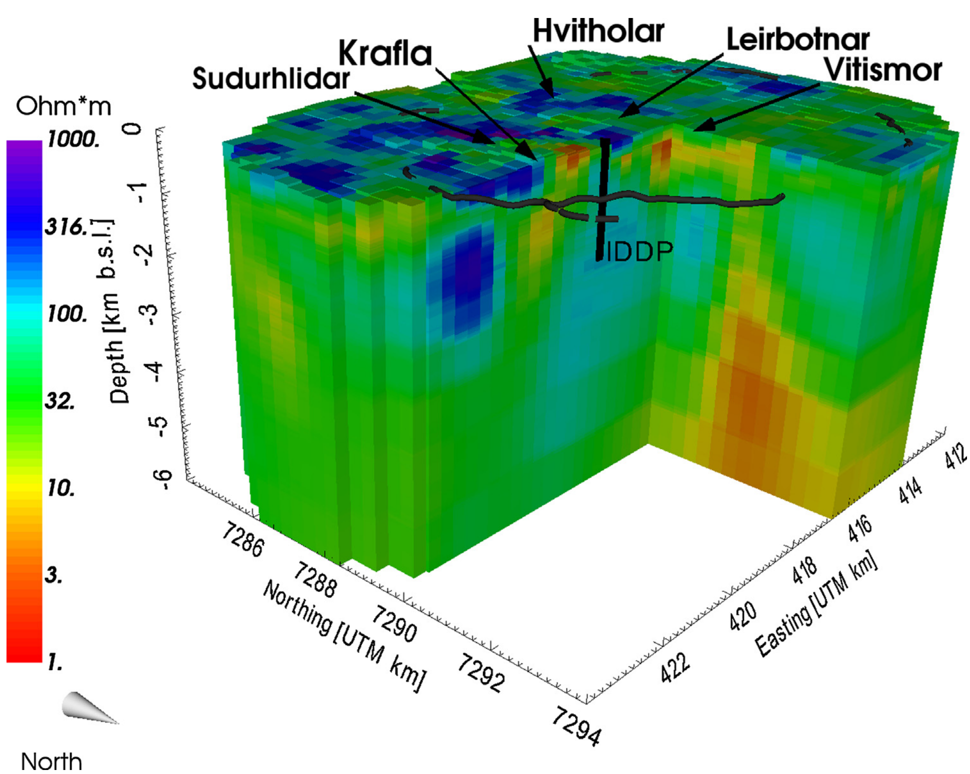

Fig. 6. 3D resistivity cut-away view at Easting = 417,000 m and Northing = 7,289,380 m from the WSINV3DMT 3D resistivity model.

et al., 2007, 2008). An active fissure swarm is 3–5 km wide and ~40 km long in a SSW-NNE direction (Fig. 7), and according to Franzson et al. (2010) it is a depression or a graben structure with large graben faults that have a total throw on the western side of more than 300 m. The faults on the eastern side have not been located as accurately but are assumed to have an overall similar throw taken up by a greater number of step-faults. Surface hydrothermal alteration is found mainly in proximity to the volcanic fissure and along a line, roughly in a SE direction, from Hengill volcano toward Hveragerdi (red symbols in Fig. 7).

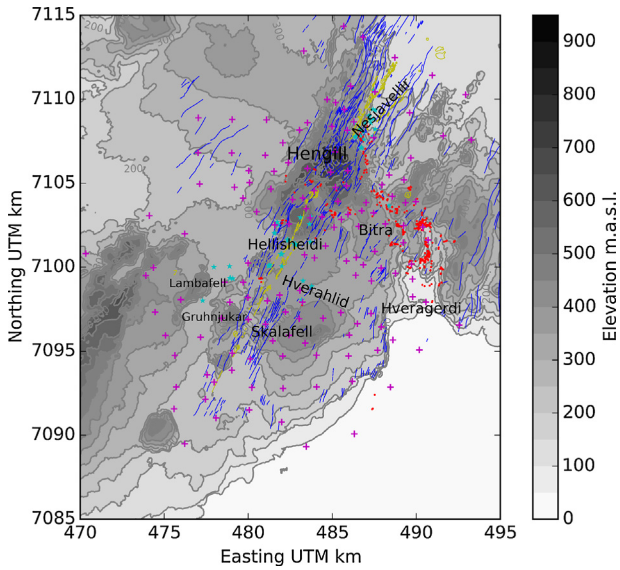

Fig. 7. Hengill elevation map with MT site (purple plus symbols) locations and labeled production fields along with the location of Mt. Hengill. Dark blue lines indicate mapped surface faults, fissures are shown in yellow, red symbols indicate surface geothermal manifestations, and cyan stars indicate drilled well locations.

At Hellisheidi, intrusions become very common below ~2 km depth (Franzson et al., 2005) and are mostly fine-grained basalts, with subordinate amounts of more evolved rock types. Periodic magmatic injections into a relatively shallow crustal environment are believed to provide the heat for the geothermal system and maintain the high geothermal gradient, though seismic evidence is lacking to confirm this hypothesis. Permeability, in general, appears to be affiliated with intrusions and sub-vertical faults/fractures. The largest part of the volcano is built up of hyaloclastite formations erupted during glacial periods, while interglacial lavas that erupted in the highlands flow to the surrounding lowlands. Franzson et al. (2010) attribute opening of new permeable pathways and the locally intensified geothermal system to Holocene volcanic fissure eruptions. This interpretation is supported by the coincidence of heating at the southern part of Nesjavellir and the location of the 5000- and 2000-year-old fissure eruption sites. Renewed heating may be caused by these eruptions because highly permeable fractures associated with the feeder dykes opened new upflow and outflow paths for the geothermal fluid, and/or because the eruption emplaced a new heat source underneath the Hengill volcano. In either case, the timing of the fissure episodes provides some constraint on the evolution of the system's temperature and hydrothermal alteration profiles, and could explain the dissonance between present-day well temperatures and MT modeling of subsurface geology at Nesjavellir. Disequilibrium between geothermal alteration and measured well temperatures is commonly observed, especially in older rocks (e.g. Kovac et al., 2005; Moore et al., 2008; Franzson et al., 2010). The geothermal system is understood to have reached peak temperature and alteration progression during the last glaciation, and has been gradually cooling since then (Franzson et al., 2010).

Fig. 7 shows elevations in the 25 km × 30 km study area and the locations of MT soundings (purple plus symbols) used in this interpretation. MT data were collected in three campaigns between 2000 and 2006. For more detailed data processing and inversion analysis, see Rosenkjaer et al. (2015).

Figs. 8 and 9 show the Hengill geothermal area 3D resistivity model with a cross-section along the SSW-NNE fissure zone. These results were obtained with the MT3Dinv inversion code. The other two inversion results are shown in Fig. 9 in Rosenkjaer et al. (2015). The northeast part of the study area (Hellisheidi, Hengill volcano, Nesjavellir, and Bitra) exhibits different resistivity behavior than the southwest part (Lambafell, Grauhnukar, Skalafell, and Hverahlid) (Fig. 9). However, both areas exhibit typical features of a high temperature geothermal system. The relationship between resistivities, well temperatures, and alteration mineralogy at Nesjavellir was shown by Arnason et al. (2010) (their Fig. 5). Unaltered cold rocks have high resistivities and low temperatures, while alteration with smectite and zeolites at low temperatures make rocks less resistive. At higher temperatures, clays contain more chlorite (or illite in more silicic rocks) and other compacted and water depleted alteration minerals (e.g., epidote) are present, which again increases resistivity. The resistive core has temperatures above 250 °C and chlorite and chlorite–epidote alteration. Variation in hydrothermal alteration mineralogy appears to be of greater importance than temperature variation for the resulting resistivity structures (Arnason et al., 2010; Haraldsdottir et al., 2012). The geothermal system could also be fossilized and, as such, retains its resistivity signature but loses its heat and geothermal fluids. A similar correlation between resistivity, temperature and alteration mineralogy has been found in all high-temperature geothermal systems in Iceland.

The inverse model identifies two low-resistivity layers: the nature of the uppermost low-resistivity layer and the increasing resistivity below it are due to hydrothermal mineral alteration, as discussed earlier. The resistivity response (Fig. 9) is consistent with the interpretation of Franzson et al. (2010): the base of the Hengill volcano is highly resistive (blue colors), representative of volcanic rocks, while areas of Hellisheidi and Nesjavellir are less resistive (green colors) at depth. The resistivity model is also in a good agreement with the Hengill reservoir model by Bjornsson et al. (2006). Very low resistivities (red and yellow colors) in the upper 1–2 km indicate the location of the clay cap. Jousset et al. (2011) and references therein show that at temperatures below 350 °C, resistivity and P-wave velocity responses in Icelandic fields are similar to the rest of the world's geothermal fields (c.f. Newman et al., 2008), in which low resistivity correlates with low permeability smectite alteration at temperatures below 200 °C. The nature of the deep low-resistivity layer in the northeast study area is not yet well understood, although it has been identified in earlier studies (Hersir et al., 1990; Oskooi et al., 2005). In our models, the low-resistivity layer is located northwest of both Mt. Hengill and Nesjavellir at ~4 km depth, and ~6–7 km below Mt. Hengill, Nesjavellir and Hellisheidi, but it does not extend underneath Bitra (Fig. 9). Hersir et al. (1990) detected a very low resistivity layer at 7.5 km depth in the Nesjavellir area, 3 km north of Mt. Hengill, which was interpreted as partial melt. Oskooi et al. (2005) also detected a very low resistivity structure at ~5 km depth southwest of Mt. Hengill, at the location of the fissure swarm, and interpreted it as either partial melt or a porous region with hot ionized fluids located on top of a magmatic heat source. Magmatic intrusions could act as a heat source for the geothermal system, although there are no seismic data to confirm the presence of magma at these locations. Low Vp/Vs ratios at depth in models by Tryggvason et al. (2002) support more the presence of supercritical fluids in pores and fractures than partially molten rocks, which contradicts the decreased resistivity seen in the MT resistivity map.

In Bitra, the geothermal system that had been gradually cooling during the last glacial period became moderately active when the Bitra lava shield erupted about 13,000 years ago. Based on geochemical, mineralogical, fluid inclusion, and formation temperature analyses, Bitra shows conclusively that the shallow and pervasive high temperature alteration was formed during the last glacial period, prior to the eruption of the Bitra formation (Franzson et al., 2010). Fig. 10 shows two cross-sections at Bitra from the 3D

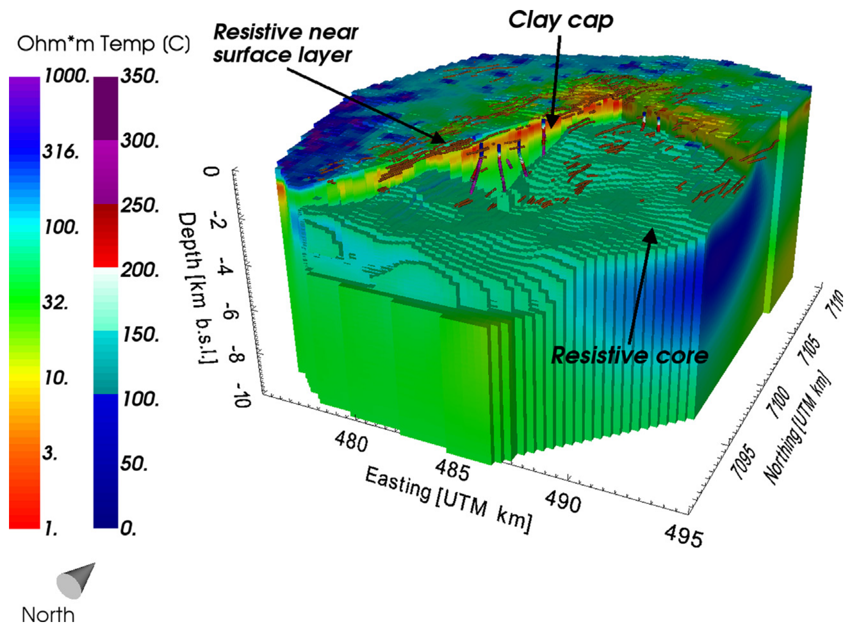

Fig. 8. 3D resistivity of the Hengill geothermal area from MT3Dinv.

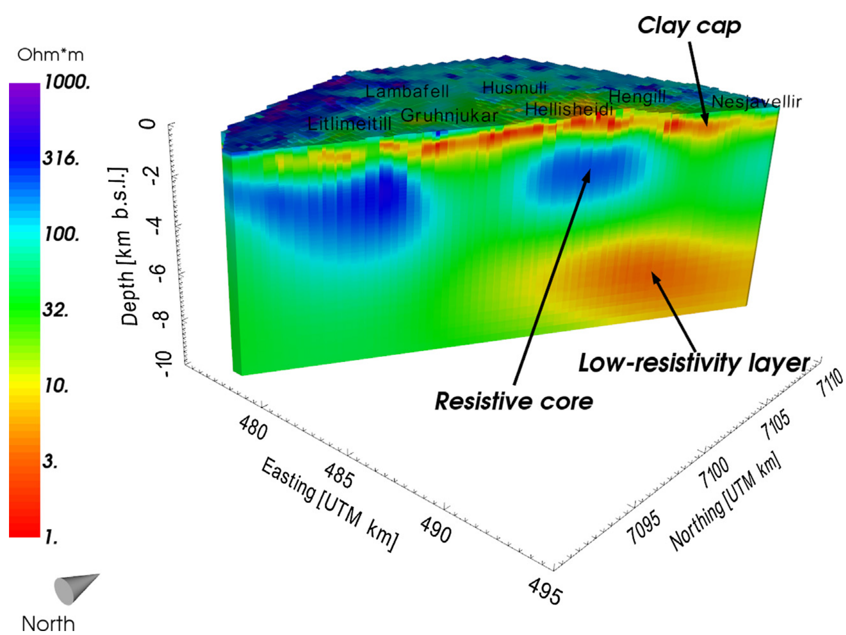

Fig. 9. 3D resistivity cut-away view along the main fissure swarm at Hengill from MT3Dinv.

resistivity model obtained with the MT3Dinv inversion code. The low resistivities in the upper 1 km are associated with hydrothermal alteration, while high resistivities down to depths of 5 km are indications of the resistive core. The cross-section parallel to the fissure swarm shows that the resistive core extends 6–9 km laterally in this direction, while the cross-section in the perpendicular direction shows its connection to the resistive core under Mt. Hengill.

A separate high-temperature system is located in the Hverahlid area to the south of the Hengill central volcano, and north of Skalafell. The Hverahlid field is somewhat different from the rest of the area, in that the stratigraphy is predominantly composed of lava successions (Helgadottir et al., 2010). This finding would suggest that the Hverahlid field was outside the main volcanism of the central volcano during glacial episodes (Franzson et al., 2010). They also note that the postglacial lavas in Hverahlid are considerably thicker than in other areas, but this system shows higher formation than alteration temperatures in the upper part indicating a Holocene heating episode similar to that found in the Hengill area. The resistivity image (Fig. 11) shows that the upper 2 km have low resistivity associated with the clay cap, but the resistive core is deeper (~3 km) than in the Skalafell area.

Helgadottir et al. (2010) show geology, formation temperatures and alteration mineralogy for a portion of our profile along the fissure swarm from Grauhnukar to Hellisheidi (Fig. 11a) (their AA′) and profile from Grauhnukar to Hverahlid (Fig. 11b) across the fissure swarm (their CC′). Again, resistivities correlate well with formation temperatures and alteration mineralogy. The transition from a low-resistivity clay cap to a high-resistivity core indicates the depth to the top of a potential geothermal reservoir. Combining

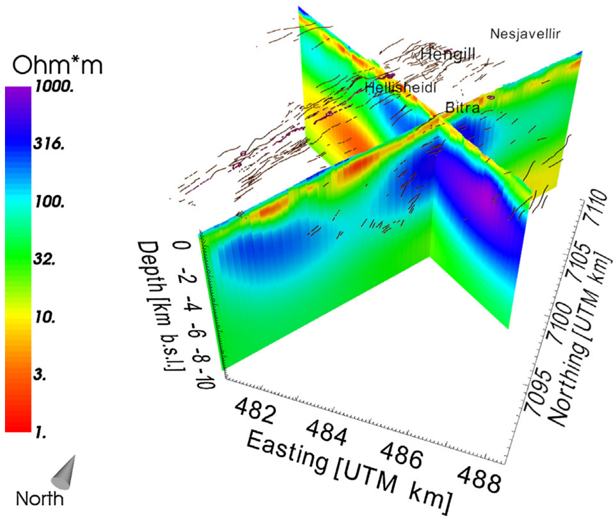

Fig. 10. Resistivity cross-sections across Bitra from MT3Dinv.

this information with other available information (e.g., geochemistry, hydrology, geology, flow simulation) leads to creation of a conceptual model (e.g. Cumming, 2009; Munoz, 2014 and references therein), which is important for resource estimation. Earlier resistivity models were incorporated into conceptual models of several geothermal fields in Hengill (e.g. Gunnarsson et al., 2010; Franzson et al., 2010). This new 3D resistivity model provides additional information that could help to refine these conceptual models, especially in the areas where are no drill holes or other measurements available.

5. Discussion

In this paper and in Rosenkjaer et al. (2015), we present 3D inversion approaches and interpretation of MT data over two geothermal areas (Krafla and Hengill). These approaches were carried out in a manner that would be used by a practitioner interested in characterizing or evaluating a potential geothermal prospect in production settings. To better and more confidently characterize the resistivity structures of the Krafa and Hengill geothermal systems, we employ three different inversion codes. These codes are run by skilled practitioners (though not the authors of the codes), and recover the same main structures reported in this paper. This is quite reassuring, suggesting that the choice of the inversion code is not the most important factor in achieving reliable results. When performing 3D inversion of MT data from a new geothermal area, the choice of the inversion code will depend on resources and on the ultimate goal of the investigation. Many times, one has to make compromises.

Once inversion results exist, we must verify that the data clearly support the model and properly resolve the features in the model. Model appraisal can be done with sensitivity studies based upon different starting models and noise assumptions in the data. Since

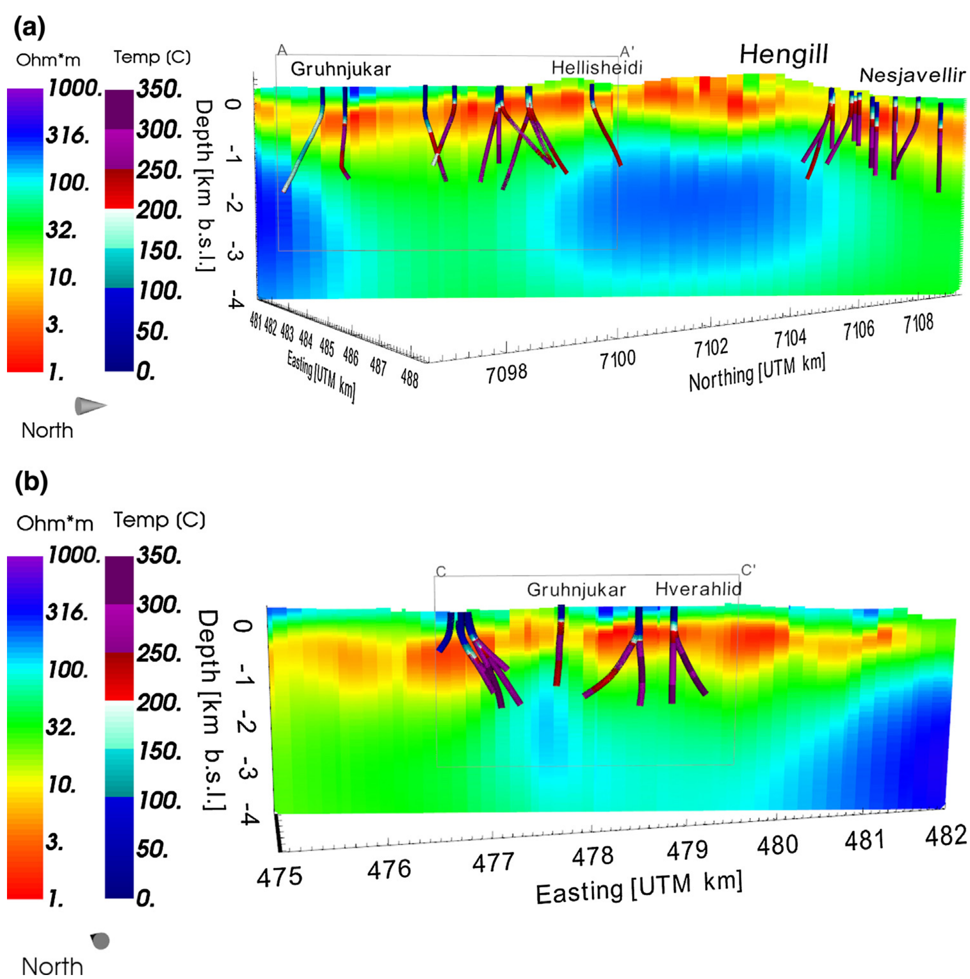

Fig. 11. (a) Resistivity cross-section along the fissure swarm from MT3Dinv and well temperatures. AA′ indicates the profile from Helgadottir et al. (2010). (b) MT3Dinv resistivity cross-section along the direction of CC′ profile from Helgadottir et al. (2010).

MT inversion is inherently non-unique, with many models fitting the data equally well, one can potentially reduce uncertainty by adding or removing a model structure and evaluating impact on the model fit to the data. This sort of resource appraisal based on MT models is very important; however in many cases we still desire independent information to further corroborate resistivity model/structure interpretations.

While this MT survey was not able to resolve individual fractures filled with magma or other fluids, for areas similar to the one at the IDDP-1 well at Krafla, where geology varies on a small spatial scale, a denser grid of MT stations and data at higher frequencies might be necessary before one could make interpretations at that scale of interest. Prior modeling of features of interest and their resolvability would further aid a survey design. MT data acquisition using continuous electromagnetic array profiling, EMAP (Torres-Verdin and Bostick, 1992), would also decrease uncertainties in interpretation resulting from static distortions. This approach is cost prohibitive at an early exploration stage, but might be worth the investment at the next stage, if a potential, much smaller, area for well siting was identified.

The near-surface structures in both areas have been thoroughly studied by many shallow geophysical measurements, geological mapping, geochemical sampling, drilling, etc. The objective of these MT surveys was to characterize deeper structures that cannot be resolved by previous surveys. The highest sounding frequency used in the inversions was 300 Hz, which is not high enough to recover variations in the upper few hundred meters, and therefore models are very different for those depths. There are not many independent measurements or information from depths below 2–3 km, so it is not possible to claim than one inversion model is better than another, or which features are true. However, getting the similar model from independent codes lends confidence that the structure is real.

In this paper we addressed capabilities and limitations of 3D MT resistivity interpretation, and where possible showed correlations with other available data. The next step would be to create a conceptual model of a geothermal system that permits the integration of disparate geologic, geochemical, geophysical, and hydrological data sets into a coherent depiction of these processes and system components (e.g. Franzson et al., 2010). Key components of geothermal systems are (1) heat source, (2) fluid flow, (3) reservoir seal (clay cap), (4) volume or resource boundaries, and (5) recharge and fluid chemistry. These components reflect major processes (such as heat and fluid flow and water–rock interaction) that control the development of hydrothermal systems. Electrical methods can be used to detect a reservoir seal that serves to retain heat and fluids within a geothermal reservoir. This seal, a low permeability clay-rich interval, resulting from hydrothermal alteration of feldspars to smectite, clearly identified in our study areas by low resistivity, is common in many geothermal systems. The top of the geothermal reservoir is located at the base of the clay-rich cap – this transition is marked by a change in alteration mineralogy from argillic to propylitic that reflects increasing temperatures. Electrical methods are also sensitive to regions of increased permeability and fluid content; therefore if the volume is above the detection threshold, resistivity could help with assessing of the fluid flow, and to some extent with evaluating the size of the heat source and resource boundaries.

An estimation of formation temperature is very important in creating a conceptual model. If fluids and/or gases are derived from a geothermal reservoir, their chemical signature can be used to indicate not only the sources of these fluids, but also to infer subsurface temperatures at which these fluids equilibrated with mineral phases in the geothermal reservoir. Alteration mineral assemblages are often diagnostic of the temperatures when they were formed. However, these assemblages might reflect the presence of a fossil hydrothermal system, or show prograde or retrograde assemblages indicative of changing thermal conditions over time (see Fig. 8 in Franzson et al., 2010).

6. Conclusions

3D MT inversions of Krafla and Hengill data sets showed that the imaging approach presented in this paper and Rosenkjaer et al. (2015) is very promising for imaging geothermal reservoirs in a single self-consistent manner, and that knowledge of the subsurface electrical resistivity can contribute to a better understanding of complex geothermal systems. Resistivity in geothermal areas is governed not only by the presence of fluid and temperature, but also by hydrothermal alteration products. Both Krafla and Hengill geothermal complexes exhibit resistivity responses similar to other high temperature geothermal areas. The resistive near-surface layer represents unaltered, relatively cold rocks, below which a low resistivity cap delineates the smectite–zeolite zone. Below this cap, a more resistive epidote–chlorite zone exists, also called the resistive core, where main production results. Resistivities in the upper 1–2 km do not correlate with lithology but with alteration mineralogy. The deep low-resistivity zone in Krafla, which varies with depth, appears to be connected to a shallow structure through vertical structures, “chimneys”. The resistivity images at the IDDP-1 well location show high resistivity, most likely a result of a combination of epidote–chlorite geology and deeper superheated steam or supercritical fluids. However, an intrusive low resistivity feature coming up from depth has been imaged about 2 km to the northwest of the well. A plausible explanation is that it represents a magma intrusion. S-wave shadow zones have been inferred in this general area four decades ago; however there was uncertainty in precisely defining its lateral boundaries. A possible explanation for the magma encounter at the IDDP-1 well is that lateral pathways or fissures connect the magma chamber to the well. The MT response to magma pathways at such scales is not observable in the existing data. Resistivity images of the Hengill geothermal area show also characteristics features of a high-temperature hydrothermal system. The nature of the uppermost low resistivity layer and the increasing resistivity below is attributed to hydrothermal mineral alteration, while the nature of the deep low-resistivity layer to the northeast is not yet well understood. Velocity models at Hengill support the presence of supercritical fluids in pores and fractures over the presence of partially molted rocks, which should lead to increases in electrical resistivity. Finally, in the Hengill southwest area, and on its east side in particular, the geothermal system appears to be deeper than that manifested to the northeast.

Acknowledgements

This work was carried out at Lawrence Berkeley National Laboratory, with funding provided by the U.S. Department of Energy Geothermal Program Office under contract GT-480010-19823-10, and Office of Basic Energy Sciences under contract DE-AC02-05CH11231. Funding for G.K. Rosenkjaer and K. Arnason was provided by Iceland Geosurvey and Geothermal Research Group GEORG. We would like to thank three anonymous reviewers for suggestions and comments that improved this manuscript.

References

Arnason, K., Magnusson, I., 2001. Geothermal activity in Hengill and in Hellisheidi, Results from resistivity measurements. Report OS-2001/091, Reykjavik (in Icelandic with English summary).

Arnason, K., Vihjalmsson, A.M., Bjornsdotttir, Th., 2009. A study of the Krafla volcano using gravity, micro-earthquake and MT data. Iceland GeoSurvey report ISOR-2009/067, Reykjavik.

Arnason, K., Eysteinsson, H., Hersir, G.P., 2010. Joint 1D inversion of TEM and MT data and 3D inversion of MT data in the Hengill area, SW Iceland. Geothermics 39, 13–34, http://dx.doi.org/10.1016/j.geothermics.2010.01.002, ISSN 0375-6505.
Axelsson, G., Egilson, T., Gylfadottir, S.S., 2014. Modelling of temperature conditions near the bottom of well IDDP-1 in Krafla, Northeast Iceland. Geothermics 49, 49–57, http://dx.doi.org/10.1016/j.geothermics.2013.05.003, ISSN 0375-6505.
Bjornsson, G., Gunnlaugsson, E., Hjartarson, A., 2006. Applying the Hengill geothermal model in power plant decision making and environmental impact studies. In: Proceedings: TOUGH Symposium 2006, Lawrence Berkeley National Laboratory, Berkeley, California, May 15–17, 2006.
Cumming, W., 2009. Geothermal resource conceptual models using surface exploration data. In: Proceedings of Thirty-Forth Workshop on Geothermal Reservoir Engineering, Stanford University, Stanford, California.
Einarsson, P., 1978. S-wave shadows in the Krafla caldera in NE-Iceland, evidence for a magma chamber in the crust. Bull. Volcanol. 41, 187–195, http://dx.doi.org/10.1007/BF02597222
Einarsson, P., 1986. Seismicity along the eastern margin of the North American Plate. In: Vogt, P.R., Tucholke, B.E. (Eds.), The Geology of North America, vol. M, The Western North Atlantic Region: Geol. Soc. Am, pp. 99–116.
Einarsson, P., 1991. Eruptions by Krofla 1975–1989. In: Einarsson, A., Gardarsson, A. (Eds.), Nature of Myvatn. The Icelandic Society of Natural Sciences, pp. 97–139 (in Icelandic).
Elders, W.A., Fridleifsson, G.O., Zierenberg, R.A., Pope, E.C., Mortensen, A.K., Gudmundsson, A., Lowenstern, J.B., Marks, N.E., Owens, L., Bird, D.K., Reed, M., Olsen, N.J., Schiffman, P., 2011. Origin of a rhyolite that intruded a geothermal well while drilling at the Krafla volcano, Iceland. Geology 39, 231–234, http://dx.doi.org/10.1130/G31393.1
Farquharson, C., Oldenburg, D., Haber, E., Shekhtman, R., 2002. An algorithm for the three-dimensional inversion of magnetotelluric data. In: 72nd SEG Annu. Meet., Salt Lake City, UT, pp. 649–652.
Foulger, G.R., Toomey, D.R., 1989. Structure and evolution of the Hengill-Grensdalur Volcanic Complex, Iceland: geology, geophysics, and seismic tomography. J. Geophys. Res.: Solid Earth 94 (B12), 17511–17522, http://dx.doi.org/10.1029/JB094iB12p17511
Franzson, H., Kristjansson, B.R., Gunnarsson, G., Bjornsson, G., Hjartarson, A., Steingrimsson, B., Gunnlaugsson, E., Grimsson, G., 2005. The Hengill-Hellisheidi geothermal field. Development of a conceptual geothermal model. In: Proceedings of the 2005 World Geothermal Congress, Antalya, Turkey, April 24–29.
Franzson, H., Gunnlaugsson, E., Arnason, K., Saemundsson, K., Steingrimsson, B., Hardarson, B.S., 2010. The Hengill Geothermal system, conceptual model and thermal evolution. In: Proceedings of the 2010 World Geothermal Congress, Bali, Indonesia, April 25–29.
Fridleifsson, G.O., Armannsson, H., Mortensen, A.K., 2006. Geothermal conditions in the Krafla caldera with focus on well KG-26, ISOR Report, ISOR-2006/030.
Fridleifsson, G.O., Armannsson, H., Gudmundsson, A., Arnason, K., Mortensen, A.K., Palsson, B., Einarsson, G.M., 2014. Site selection for the well IDDP-1 at Krafla. Geothermics 49, 9–15.
Gunnarsson, G., Arnaldsson, A., Oddsdottir, A.L., 2010. Model simulations of the geothermal fields in the Hengill Area, South-Western Iceland. In: Proceedings of the 2010 World Geothermal Congress, Bali, Indonesia, April 25–29.
Haraldsdottir, S.H., Franzson, H., Arnason, K., SGP-TR-194 2012. Preliminary study of down-hole resistivity from 72 boreholes in the S-Hengill geothermal field, SW Iceland, with respect to surface resistivity data and alteration minerals. In: Proceedings of Thirty-Seventh Workshop on Geothermal Reservoir Engineering Stanford University, Stanford, California, January 30–February 1, 2012.
Hardarson, B.S., Helgadottir, H.M., Franzson, H., 2007. The Hellisheidi power plant. The injection area by Grauhnukar, Report, ISOR-2007/001 (in Icelandic).
Hardarson, B.S., Mortensen, A.K., Einarsson, G.M., Franzson, H., 2008. Hole HN-9 and the disposal of waste-water from the Hellisheidi power plant by Kolvidarhol, Report, ISOR-2008/006 (in Icelandic).
Helgadottir, H.M., Snaebjornsdottir, S.O., Nielsson, S., Gunnarsdottir, S.H., Matthiasdottir, T., Hardarson, B.S., Einarsson, G.M., Franzson, H., 2010. Geology and hydrothermal alteration in the reservoir of the Hellisheidi high temperature system, SW-Iceland. In: Proceedings of the 2010 World Geothermal Congress, Bali, Indonesia, April 25–29.
Hersir, G.P., Bjornsson, G., Bjornsson, A., 1990. Eldstodvar of jardhiti a Hengilssvaedi, Jardedlisfraedileg konnun (Volcanoes and geothermal resources in the Hengill area, geophysical research). Nat. Energy Auth., Iceland, Re OS-90031/JHD-06.
Jousset, P., Haberland, Ch., Bauer, K., Arnason, K., 2011. Hengill geothermal volcanic complex (Iceland) characterized by integrated geophysical observations. Geothermics 40, 1–24, http://dx.doi.org/10.1016/j.geothermics.2010.12.008
Kovac, K.M., Moore, J.N., Lutz, S.J., 2005. Geologic framework of the East Flank, Coso geothermal field: implications for EGS development. In: Proceedings of Thirtieth Workshop on Geothermal Reservoir Engineering, Stanford University, Stanford, California.
Madden, T.R., Nelson, P., 1986. A defense of Cagniard's Magnetotelluric Method. In: Vozoff, K. (Ed.), Magnetotelluric Methods, Geophysics Reprint Series No. 5, Soc. Explor. Geophys, pp. 89–102.
Moore, J.N., Allis, R.G., Nemcok, M., Powell, T.S., Bruton, C.J., Wannamaker, P.E., Raharjo, I.B., Norman, D.I., 2008. The evolution of volcano-hosted geothermal systems based on deep wells from Karaha-Telaga Bodas, Indonesia. Am. J. Sci. 308, 1–48.
Mortensen, A.K., Gronvold, K., Gudmundsson, A., Steingrimsson, B., Egilson, T., 2010. Quenched silicic glass from well K-39 in Krafla, North-Eastern Iceland. In: Proceedings of the 2010 World Geothermal Congress, Bali, Indonesia, April 25–29.
Munoz, G., 2014. Exploring for geothermal resources with electromagnetic methods. Surv. Geophys. 35, 101–122, http://dx.doi.org/10.1007/s10712-013-9236-0
Newman, G.A., Alumbaugh, D.L., 2000. Three-dimensional magnetotelluric inversion using non-linear conjugate gradients. Geophys. J. Int. 140, 410–424.
Newman, G.A., Recher, S., Tezkan, B., Neubauer, F.M., 2003. 3D inversion of a scalar radio magnetotelluric field data set. Geophysics 68, 782–790.
Newman, G.A., Gasperikova, E., Hoversten, G.M., Wannamaker, P.E., 2008. 3D magnetotelluic characterization of the Coso geothermal field. Geothermics 37, 369–399.
Oskooi, B., Pedersen, L.B., Smirnov, M., Arnason, K., Eysteinsson, H., Manzella, A., the DGP Working Group, 2005. The deep geothermal structure of the Mid-Atlantic Ridge deduced from MT data in SW Iceland. Phys. Earth Planet. Int. 150, 183–195.
Pellerin, L., Johnston, J.M., Hohmann, G.W., 1996. A numerical evaluation of electromagnetic methods in geothermal exploration. Geophysics 61, 121–130.
Rosenkjaer, G.K., Gasperikova, E., Newman, G.A., Arnason, K., Lindsey, N.J., 2015. Comparison of 3D MT inversions in geothermal exploration. Case studies for Krafla and Hengill geothermal systems in Iceland. Geothermics 57, 258–274.
Siripunvaraporn, W., 2011. Three-dimensional magnetotelluric inversion: an introductory guide for developers and users. Surv. Geophys. 33, 5–27.
Spichak, V.V., Zakharova, O.K., 2014. Gaseous vs. aqueous fluids: Travale (Italy) case study using EM geothermometry. In: Proceedings of the Thirty-Ninth Workshop on Geothermal Reservoir Engineering, Stanford, California, February 24–26, 2014, SGP-TR-200.
Torres-Verdin, C., Bostick Jr., F.X., 1992. Principles of spatial surface electric field filtering in magnetotellurics: electromagnetic array profiling (EMAP). Geophysics 57, 603–622.
Tryggvason, A., Rognvaldsson, S.Th., Flovenz, O.G., 2002. Three-dimensional imaging of the P- and S-wave velocity structure and earthquake locations beneath Southwest Iceland. Geophys. J. Int. 151, 848–866.
Vozoff, K., 1991. The magnetotelluric method. In: Nabighian, M.N. (Ed.), Electromagnetic methods in applied geophysics, vol. 2B. Soc. Explor. Geophys., Tulsa, pp. 641–711.